Applied Catalysis B: Environmental 90 (2009) 29–37

Contents lists available at ScienceDirect

Applied Catalysis B: Environmental

journal homepage: www.elsevier.com/locate/apcatb

Steam reforming of glycerol: The experimental activity of $La_{1-x}Ce_xNiO_3$ catalyst in comparison to the thermodynamic reaction equilibrium

Y. Cui, V. Galvita, L. Rihko-Struckmann *, H. Lorenz, K. Sundmacher

Max Planck Institute for Dynamics of Complex Technical Systems, Sandtorstr. 1, 39106 Magdeburg, Germany

ARTICLE INFO

Article history:
Received 1 September 2008
Received in revised form 11 February 2009
Accepted 13 February 2009
Available online 21 February 2009

Keywords:
Glycerol
1,2,3-Propantriol
Hydrogen
Steam reforming
Mixed oxide
$La_{1-x}Ce_xNiO_3$

ABSTRACT

The steam reforming of glycerol (1,2,3-propantriol) was investigated with non-substituted and partially Ce substituted $La_{1-x}Ce_xNiO_3$ mixed oxides where $x = 0$, 0.1, 0.3 or 0.7, and the activities were compared with Pt metal catalysts. The catalysts were characterised by temperature-programmed reduction (TPR), X-ray powder diffraction (XRD), BET surface area and carbon content. The Ni was easily reduced in the $La_{0.3}Ce_{0.7}NiO_3$ structure. The experimental results were compared with the thermodynamic equilibrium concentrations, which were calculated for the system with non-stochiometric method. The $La_{0.3}Ce_{0.7}NiO_3$ catalyst was highly active in the glycerol steam reforming with conversions approaching to the equilibrium at temperatures between 500 and 700 °C. The formation of carbonaceous deposits on the $La_{0.3}Ce_{0.7}NiO_3$ was smallest among all the investigated $La_{1-x}Ce_xNiO_3$ catalysts. Unchanged catalyst surface area (BET) during operation and low carbon deposition after reaction confirm the efficient operation and high stability of the non-noble, inexpensive catalyst of $La_{0.3}Ce_{0.7}NiO_3$.

1. Introduction

The interest on the conversion of biomass to hydrogen has increased considerably during the last years. Hydrogen gas has been identified as an ideal energy carrier for sustainable energy supply and it would be an ideal fuel in all fuel cell types to generate electricity with high efficiency [1–4]. In the short term, natural gas is the most viable and inexpensive source for large scale hydrogen production [5], but the reforming of it does not contribute to the reduction of greenhouse gases. Therefore, the production of hydrogen from non-fossil sources (especially from biomass [6]), would have higher environmental impact as it would lower the overall greenhouse gas emissions. Among the various non-fossil feedstock source, glycerol (1,2,3-propantriol) is one alternative because it has a relatively high hydrogen content, it is non-toxic, and its storage and handling is safe. More importantly, glycerol is the main byproduct in the production of the first generation biodiesel made by the transesterification of vegetable oils. The worldwide production of glycerol was more than 0.9 million tons in 2006, and in 2010 its production is estimated to be as high as 1.2 million tons [7]. The recent reviews of Johnson and Taconi [7] and Behr et al. [8] provide excellent overviews of the chemistry of glycerol, and its possible utilisation as renewable resource not only for the production of various chemicals but also for the production of synthesis gas.

Aqueous phase reforming of glycerol has been extensively investigated by Dumesic and co-workers [9–11]. Moreover, some experimental studies of photocatalytic [12] and gas phase steam reforming of glycerol [13–20] have been published recently. The aqueous phase reforming of glycerol necessitates the utilisation of high pressure, which decreases the selectivity of hydrogen compared to the gas phase steam reforming of glycerol under atmospheric pressure [9,19]. The formation rate of hydrogen in the photocatalytic conversion of glycerol is considerably lower than that in gas phase steam reforming of glycerol [12,19]. Furthermore, steam reforming is highly energy efficient technology, and it can be carried out at atmospheric pressure. The steam reforming of glycerol has similarities to the reforming of light alcohols: methanol [21–26] and ethanol [2,6,27–37] reforming has intensively been investigated experimentally with various catalysts, e.g. with unpromoted and Ce–Zn-promoted Cu, Ni, Rh, Pd, Co, Ir, Ni on carriers such as CeO_2, CeO_2/ZrO_2 or alumina. Ni is also the most investigated active metal in the glycerol reforming, due to its well known property to promote the necessary C–C rupture [15–18]. However, in some comparative studies, other metals, e.g. Ru, Ir and Rh have shown even higher activity than Ni [16–17,19–20]. In the primary investigation of Suzuki and co-workers [19], Ru/Y_2O_3 catalyst was found to have the high activity in the gas phase steam reforming. On the other hand, Ce containing catalysts are known to have high oxygen storage capacity, to disperse the active metal

* Corresponding author. Tel.: +49 391 6110318; fax: +49 391 6110566.
E-mail address: rihko@mpi-magdeburg.mpg.de (L. Rihko-Struckmann).

0926-3373/$ – see front matter © 2009 Elsevier B.V. All rights reserved.
doi:10.1016/j.apcatb.2009.02.006

efficiently and to inhibit sintering. Furthermore, Ce is known to promote the water-gas-shift reaction and to facilitate gasification of carbon matter [6]. Based on these desired properties of Ce, its influence has been found to be highly positive in the glycerol reforming [16–18]. Rh catalysts with the addition of ceria washcoat covered alumina foam was found to be active in the autothermal reforming of various volatile carbohydrates, e.g. glycerol, both in the absence of water, steam to carbon ratio (S/C) being zero, as well in the steam reforming conditions (S/C ratio 4.5) by Dauenhauer et al. [20]. With steam to carbon ratio of 4.5 and carbon/oxygen ratio of 1.6, the hydrogen selectivity was 115% meaning that hydrogen from the co-fed steam was also partially converted to gaseous dihydrogen. In the present study, we investigated a new type of catalyst, Ce substituted $LaNiO_3$ mixed oxide, containing Ni as active metal.

There are several ways to produce hydrogen from carbohydrates, which have the general formula $C_n(H_2O)_nH_2$. Due to the high oxygen content of the carbohydrate molecule itself, oxygen is inevitably present in the systems where carbohydrates are involved. The conversion to synthesis gas is therefore possible even through decomposition reaction as written for glycerol in the Eq. (1):

$$C_3(H_2O)_3H_2 \rightarrow 3CO + 4H_2 \quad (1)$$

According to Eq. (1), maximally four moles of hydrogen per one mole of glycerol ($n = 3$) can be formed via simple decomposition. In the steam reforming conditions, however, the water-gas-shift reaction will occur simultaneously, and therefore maximally seven moles of hydrogen could be generated in the steam reforming of glycerol (see Eq. (2)):

$$C_3(H_2O)_3H_2 + 3H_2O \rightarrow 3CO_2 + 7H_2 \quad (2)$$

However, the yield of hydrogen in this system is controlled by the thermodynamics. It is well known that at higher temperatures the reaction equilibrium turns to be unfavourable for the water-gas-shift reaction and the reverse reaction is more intensive, and therefore the yield of hydrogen reaches a maximum in the optimum temperature range. The estimation of the thermodynamic equilibria of the system containing glycerol is carried out in the present study. However, the thermodynamic calculations of glycerol systems should be taken indicative as the physico-chemical behaviour of glycerol is far from ideal, and the decomposition of the molecule likely occurs at moderate temperatures. Furthermore, the reliability of the numeric values for the thermodynamic properties, ΔH_f and ΔG_f, which are needed in the thermodynamic calculation, could not be confirmed from several sources.

The goal of the present study was to estimate the thermodynamic equilibria and the equilibrium composition of the system containing glycerol, CO, H_2O, CO_2, H_2 and CH_4 as a function of temperature and steam to carbon ratio. Furthermore, the conversion of glycerol and the yield of hydrogen in the steam reforming conditions were investigated experimentally with $La_{1-x}Ce_xNiO_3$ mixed oxides catalysts.

2. Experimental

2.1. Thermodynamic analysis of the system containing glycerol

The thermodynamics of the system containing glycerol in the steam reforming conditions was analyzed initially. The equilibrium composition of the system is calculated as a function of the reaction temperature and the steam to carbon (S/C) ratio.

In the glycerol steam reforming, H_2, H_2O, CO_2, and CO aside of the feed polyalcohol are assumed to be thermodynamically possible components. Methane, which is thermodynamically highly stable even at high temperature, and of which existence has been confirmed in the steam reforming of ethanol [35–37], is also included in the calculations for glycerol steam reforming. The equilibrium gas composition of any reacting system can be calculated either by stoichiometric [38] or non-stochiometric approach [39–41]. In the non-stochiometric method one does not need to specify any set of reactions occurring in the system, and the equilibrium composition is calculated by the minimisation of the total Gibbs free energy of the system [40,41]. This simple method was applied here as it enables the calculation of the gas composition of any reacting system, and it does not necessitate any initial estimation of the equilibrium.

The total Gibbs free energy of a system is written as a sum of the Gibbs free energies of the system species:

$$G^t = \sum_{i=1}^{N} n_i \overline{G_i} = \sum_{i=1}^{N} n_i \mu_i = \sum n_i {G_i}^{\theta} + RT \sum n_i \ln \frac{\hat{f}_i}{{f_i}^{\theta}} \quad (3)$$

where G^t is the total Gibbs free energy and n_i is the moles of species i. For reaction equilibrium in the gas phase, $\bar{G}_i$ is the partial molar Gibbs free energy of species i, μ_i the chemical potential, R the molar gas constant, G_i^{θ} the standard Gibbs free energy, T the temperature of system, and $\hat{f}_i$ the fugacity of the species i in the system. The fugacity in the vapor phase is defined excluding the Poynting factor as $\hat{f}_i = y_i \hat{\phi} P$, where y_i is the gas phase mole fraction of species i, $\hat{\phi}_i$ the fugacity coefficient of species i and P the pressure of system. For a system at low pressure we might assume here that the fugacity coefficient $\hat{\phi}_i$ is close to one. It is further assumed that the standard-state fugacity $f_i^{\theta} = p^{\theta}$, where P^{θ} is the standard pressure of 101.3 kPa, and ${G_i}^{\theta} = \Delta G_{f_i}^{\theta}$. By using the Lagrange multiplier method for the minimisation of Eq. (3), the minimum Gibbs free energy of each gaseous species and that of the total system can be expressed as Eqs. (4) and (5), respectively.

$$\Delta G_{f_i}^{\theta} + RT \ln \frac{y_i \hat{\phi}_i P}{P^{\theta}} + \sum_k \lambda_k a_{ik} = 0 \quad (4)$$

$$\sum_{i=1}^{N} n_i \left(\Delta G_{f_i}^{\theta} + RT \ln \frac{y_i \hat{\phi}_i P}{P^{\theta}} + \sum_k \lambda_k a_{ik} \right) = 0 \quad (5)$$

where the constraining Eq. (6) is obtained from the balances:

$$\sum_i n_i a_{ik} = A_k \quad (6)$$

In the above equations, $\Delta G_{f_i}^{\theta}$ is the standard Gibbs function of formation of species i, λ_k the Lagrange multiplier, a_{ik} the number of atoms of the kth element present in each molecule of species i, and A_k the total mass of kth element in the feed. The minimum of the Gibbs enthalpy of the system, and the concentrations of the components n_i at that the point were determined with the Matlab solver fmincon. The thermodynamic data used in our study was obtained mostly from [42]. For glycerol, the liquid phase value of Gibbs free energy of formation, $\Delta G_{f_i}^{\theta}$ (−477.0 kJ/mol) [43] was used in the equilibrium calculations below.

2.2. Catalyst synthesis

The $La_{1-x}Ce_xNiO_3$ mixed oxide catalysts were prepared by the co-precipitation method. The catalysts were synthesized from the corresponding nitrates: $Ce(NO_3)_3{\cdot}6H_2O$ (99.0%, Fluka) and $La(NO_3)_3{\cdot}6H_2O$ (99.0%, Fluka) and $Ni(NO_3)_2{\cdot}6H_2O$ (99.0%, Fluka), which were dissolved in distilled water. The ratio between the metal salts was altered depending on the desired La/Ce molar ratio: $La_{1-x}Ce_xNiO_3$ where $x = 0$, 0.1, 0.3, or 0.7. The precipitation was carried out by adding ammonium hydrogen carbonate solution to

the nitrate solution during rigorous mixing. The resulting precipitate was filtered, washed with distilled water, dried at 100 °C for 4 h. After that the oxide material was carefully ground in a mortar, and subsequently calcined at 900 °C for 6 h. The catalyst particles were finally prepared by pressing the calcined material to plates, crushing the plates, and sieving the fraction between 280 and 560 μm.

2.3. Catalyst characterization

The BET surface areas of the samples were determined by N_2 adsorption at −196 °C by Quantachrom Instruments NOVA 2000e equipment (Quantachrom, Germany). Prior to the analysis, the samples were outgassed in vacuum at 250 °C for 4 h on order to remove any volatile adsorbents on the surface.

The phase analysis of the materials was performed using X'Pert PRO powder diffractometer equipped with an X'Celerator detector (both from PANalytical, Germany) using standard Cu Kα radiation. The powder diffraction patterns were collected in a 2θ scan range from 10° to 80° and a step size of 0.008° with 50 s counting time at each angle. The Powder Diffraction File (PDF 2.0 set 53, 2003) from the International Center for Diffraction Data (ICDD) was used to identify the crystalline phases present in the samples. The average particle size of Ni crystallites was determined by comparing the width of a standard profile (LaB_6, NIST-Standard 660a) with the sample profile according to the Scherrer formula. Spherical shape was assumed for the crystallites. The elementary contents (La, Ce, Ni) in the catalysts were determined with ICP/OES.

The reducibility of the prepared catalysts was investigated by temperature-programmed reduction (TPR) method in BEL-CAT Catalyst Testing Equipment (Rubotherm, Germany). About 100 mg of catalyst was placed in an U-shaped quartz tube and pretreated in He stream of 30 ml/min at 400 °C for 30 min prior to running the TPR experiment, and then cooled down to room temperature in He. The feed of 10% H_2 in He at a flow rate of 30 ml/min was used as reducing gas. The temperature was increased with a constant rate of 15 °C/min. The hydrogen consumption was monitored using a thermal conductivity detector.

2.4. Catalytic activity

The catalytic activity of the prepared mixed oxides $La_{1-x}Ce_xNiO_3$ (x = 0, 0.1, 0.3, 0.7) in the steam reforming of glycerol was investigated under atmospheric pressure. The measurements were carried out in a horizontally located tubular quartz microreactor (i.d. 10 mm, 300 mm length). The water/glycerol mixture was vaporized in the first part of the reactor which was filled with quartz wool. The mixed oxide catalyst (100 mg) having particle size between 280 and 560 μm was packed between layers of quartz wool and was located in the reactor at a position 2/3 of the whole length, whereas the last 1/3 part of the reactor was filled with inert aluminium oxide (α-Al_2O_3). The reactor was placed in an electric furnace equipped with K-type thermocouples. The temperature of the catalyst layer was measured by a thermocouple located inside of the reactor at the position of the catalysts bed. The liquid mixture flow rate of the $H_2O/C_3H_8O_3$ mixture was controlled with a Hamilton Microlab microsyringe pump with syringe volume 250 μm and was kept constant at 0.06 ml/min in all investigations. The steam to carbon ratio (S/C) defined as the moles of water divided by the moles of atomic carbon was in all investigations 8 ($H_2O/C_3H_8O_3$ molar ratio 24:1). The carrier gas Ar was kept constant at 33 ml/min by Brooks mass flow controller. Prior to an activity test, the catalyst was reduced at 700 °C under a gas flow (33 ml/min) with reducing gas mixture containing 10% H_2 in Ar for 30 min. After the reduction phase, the activity was measured at temperatures 500, 550, 600 and 700 °C. The gas concentrations at each condition (e.g. temperature) were measured at least by three gas chromatographic analyses with an analysis time of 30 min each, and the duration time at one condition was typically 2.5–3 h. A complete test with one catalyst investigated at four temperatures took about 14 h.

The product stream from the reactor outlet was passed through a cold trap (0 °C) in order to condense water and unreacted glycerol, and the permanent gases (H_2, CO_2, CO, CH_4, C_2H_4, C_2H_6, Ar) were led further into a gas chromatograph. The quantitative analyses of the gaseous products were carried out with Agilent gas chromatograph equipped with TCD (Model 6890). Packed columns MS5Å and PPQ were used for component separation and Ar as carrier gas. The concentration of glycerol was analyzed with a HPLC chromatograph Dionex equipped with Lichrocart-250-4 column filled with Lichrospher 100-NH_2 (5 μm) and UV-detector. Traces of other hydrocarbons presented in the collected trap liquid were detected in the HPLC analysis, but they were not identified.

The conversion of glycerol to gaseous products CO_2, CO, CH_4, C_2H_4 and C_2H_6 was calculated according to Eq. (7)

$$X_g\,(\%) = \frac{F_{out}\cdot([CO_2]+[CO]+[CH_4]+2\cdot[C_2H_4]+2\cdot[C_2H_6])}{F_{in}\cdot 3[C_3H_8O_3]_{in}}\cdot 100\% \quad (7)$$

where F_{out} is the product gas rate (mol/min), F_{in} the molar feed rate (mol/min); $[CO_2]$, $[CO]$, $[CH_4]$, $[C_2H_4]$, $[C_2H_6]$ and $[C_3H_8O_3]$ are the concentrations of CO_2, CO, CH_4, C_2H_4, C_2H_6 and $C_3H_8O_3$, respectively.According to the stoichiometry of the reforming reaction presented in Eq. (2), the yield of hydrogen is calculated by Eq. (8):

$$\text{Hydrogen yield}\,(\%) = \frac{[H_2]\cdot F_{out}}{7\cdot n_{gly,in}}\cdot 100\% \quad (8)$$

Fractional conversion of a carbon molecule in the feed to a gaseous product is calculated by Eq. (9):

$$X_M = \frac{F_{out}\cdot[M]}{F_{in}\cdot 3[C_3H_8O_3]_{in}} \quad (9)$$

where [M] is the concentration of CO_2, CO, CH_4.

3. Results and discussion

3.1. Results of the thermodynamic analysis

Similarly as for the lighter hydrocarbons, the following reactions likely occur in the steam reforming of glycerol:

$$C_3H_8O_3 \Leftrightarrow 4H_2 + 3CO \quad (\text{directdecomposition}) \quad (10)$$

$$CO + H_2O \Leftrightarrow H_2 + CO_2 \quad (\text{WGS}) \quad (11)$$

$$CO + 3H_2 \Leftrightarrow CH_4 + H_2O \quad (\text{methanation}) \quad (12)$$

$$CH_4 + H_2O \Leftrightarrow CO + 3H_2 \quad (CH_4\ \text{steam reforming}) \quad (13)$$

$$CH_4 + CO_2 \Leftrightarrow 2CO + 2H_2 \quad (CH_4\ \text{dry reforming}) \quad (14)$$

The thermodynamic analysis indicates that glycerol is completely converted in the temperature range of 250–850 °C for S/C ratios between 1 and 5. Fig. 1 illustrates the amount of hydrogen in equilibrium calculated per mole glycerol with S/C ratios from 1 to 5. As seen in the figure, the amount of hydrogen in equilibrium is dependent not only on the temperature but also from the S/C ratio. The amount of hydrogen in equilibrium increases as a function of temperature from 250 to 600 °C (depending slightly on the initial steam to carbon ratio). Above this temperature the amount of

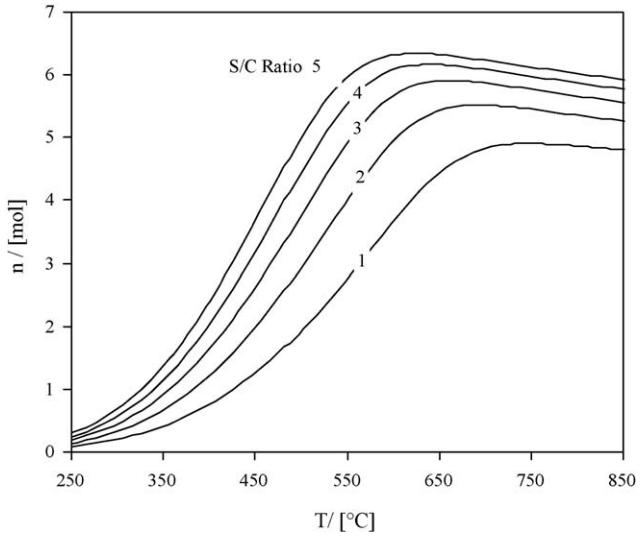

Fig. 1. The amount of hydrogen in the thermodynamic equilibrium calculated per mole glycerol with steam to carbon ratios (S/C) from 1 to 5.

hydrogen gradually decreases. The amount of hydrogen increases as a function of the S/C ratio, and the S/C ratio influences on the temperature where the highest yield of hydrogen is obtained. For example, the maximum amount of hydrogen (4.90 mol/mol_{gly}) is obtained at 750 °C with S/C ratio 1, and (6.33 mol) at 630 °C with S/C ratio 5. Above the temperatures of 630 °C it is likely that the more intensive influence of the reverse water-gas-shift reaction decreases the amount of hydrogen, as similarly the concentration of CO increases and the concentration of CO_2 decreases. Methane is stable in the system at the low temperatures, but its amount decreases strongly as a function of temperature, and it is negligible at temperatures above 730 °C. The mole fractions of H_2O, H_2, CO, CO_2, CH_4 in the thermodynamic equilibrium as a function of temperature are illustrated in Fig. 2. Glycerol is not stable at this temperature range. The mole fraction of each component *i* in the product stream, x_i is calculated with the equation $n_i/(nCO + nCO_2 + nH_2 + nCH_4 + nH_2O)$. As seen in Fig. 2, at temperature above 530 °C, the main component aside water is hydrogen, but its mole fraction remains always below 0.5, even with the lowest calculated steam to carbon ratio. The increased steam to carbon ratio decreases the concentration of CO considerably. The obtained results are in full agreement with the recent results of Adhikari et al. [15,44], which are based also on the calculation method of Gibbs energy minimisation.

3.2. Characterization of the $La_{1-x}Ce_xNiO_3$ catalysts

The BET surface areas of calcined and used catalysts are shown in Table 1. The ceria substitution of $LaNiO_3$ increased the surface area of the investigated catalyst: from $La_{0.9}Ce_{0.1}NiO_3$, to $La_{0.3}Ce_{0.7}NiO_3$ the surface area increased from 12.6 to 20.0 m^2/g, respectively. The highest surface area was measured in the fresh catalyst with highest substitution degree, $x = 0.7$. The high substitution level of La with Ce improved also the stability against sintering in the reactor conditions of simultaneous high steam concentration and high temperature, as for $La_{0.3}Ce_{0.7}NiO_3$ and $La_{0.7}Ce_{0.3}NiO_3$ only 1–2% decrease of the surface area was observed after about 10 h of operation. For the lowest investigated substitution degree, $x = 0.1$, in $La_{0.9}Ce_{0.1}NiO_3$, a decrease of 17.9% was observed in the surface area after operation.

Table 1 lists the carbon content of the $La_{1-x}Ce_xNiO_3$ catalyst as well. The initial carbon content 0.3 wt% was determined from an unused sample $La_{0.3}Ce_{0.7}NiO_3$, and due to the equal synthesis

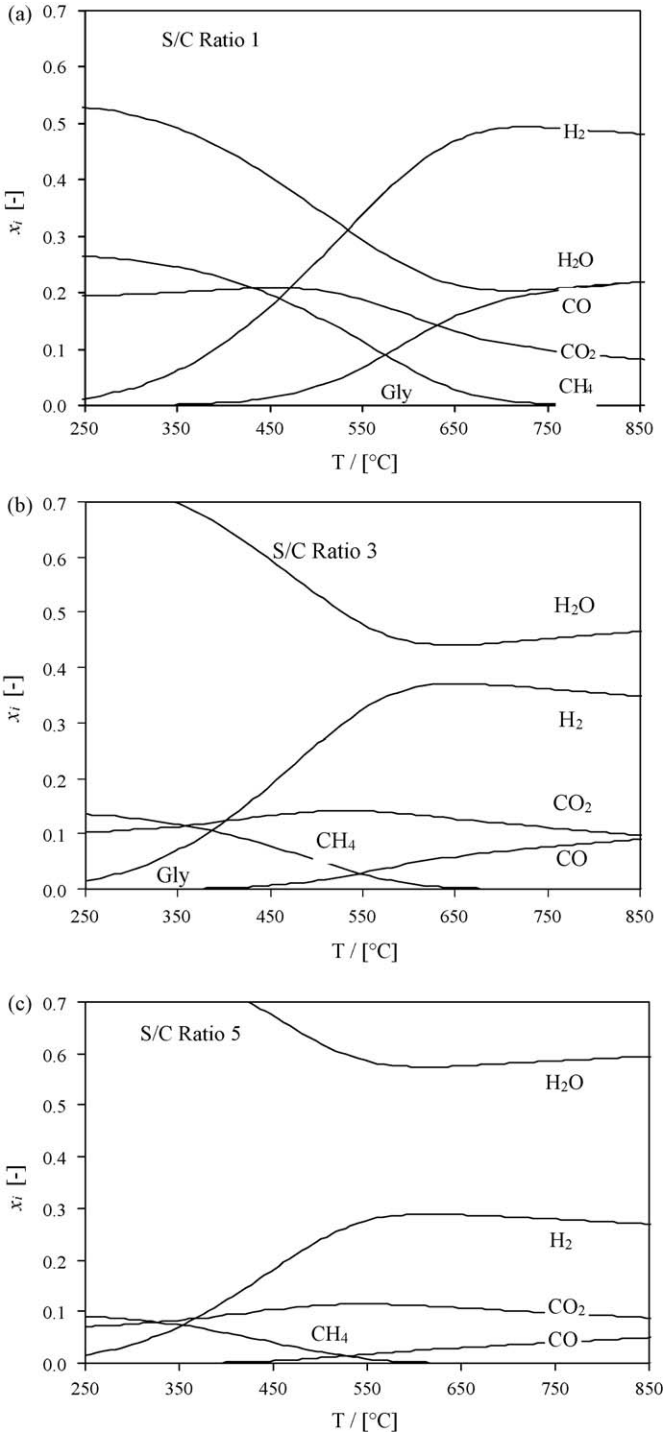

Fig. 2. The mole fractions of H_2, CO, CO_2, CH_4, $C_3H_8O_3$ in the thermodynamic equilibrium as a function of temperature with steam to carbon ratio (S/C): (a) 1, (b) 3 and (c) 5.

Table 1
The surface area and carbon content of the fresh and used $La_{(1-x)}Ce_xNiO_3$ catalysts.

	BET (m^2/g)		C content (wt%)	
	Fresh	Used	Fresh	Used
$La_{0.9}Ce_{0.1}NiO_3$	12.6	10.4		1.70
$La_{0.7}Ce_{0.3}NiO_3$	13.3	13.2		1.90
$La_{0.3}Ce_{0.7}NiO_3$	20.0	19.7	0.3	0.60

method similar initial values are likely for the other materials as well. As seen in Table 1, the catalyst with the substitution degree, $x = 0.7$, had not only the highest surface area as fresh and used catalyst but had also considerably lower tendency for coking than the two other investigated Ce substitution degrees $x = 0.1$ and 0.5. For the $La_{0.3}Ce_{0.7}NiO_3$ a carbon content of 0.6 m% was measured after the operation as for the other the level of coking was in the range between 1.7 and 1.9 wt%. The catalyst $La_{0.3}Ce_{0.7}NiO_3$ seems to be highly resistant against carbon deposition. This is in agreement with literature [17] where Ce supported metal catalysts showed high resistance against coking in glycerol steam reforming. In our studies, the BET results indicate that the substitution of Ce promotes the stability of the catalysts surface area.

The elementary composition of the prepared mixed oxides likely depends on the synthesis conditions, and the elementary composition of identical samples was found to vary to some extent. The La contents of the samples were close to the nominal one, being 61, 53, 45 and 22% with the substitution level $x = 0$; 0.1; 0.3; 0.7, respectively. Ni content of the samples was typically between 19 and 22%. However, in the samples with the nominal composition of $La_{0.3}Ce_{0.7}NiO_3$ the Ni content was below 10 wt%, and the ceria content respective higher.

3.3. Reduction of $La_{1-x}Ce_xNiO_3$ catalysts (TPR)

Since active sites for the glycerol steam reforming reaction are Ni^0 crystallites, the activation of the oxide precursors in a reducing atmosphere must be done prior to reaction. The TPR experiments were performed in order to investigate the reducibility of the prepared mixed oxides catalysts. The changes in the reduction ability indicate changes in the catalytic activity caused by the ceria addition in the material. The reduction of the four investigated samples without ceria and with substitution $x = 0$; 0.1; 0.3; 0.7 (Fig. 3) occurred over several steps as several peaks were observed during the TRP analysis, which likely correspond to different intermediary species of Ni, CeO_2, and La_2O_3. For comparison, the TPR profiles of NiO and CeO_2 are added as well in the illustration, but as seen in Fig. 3 no clear peaks were obtained with CeO_2. The unsubstituted $LaNiO_3$ sample was reduced in three steps, as the maximum of the peaks appeared at 375, 510 and 610 °C. The peaks can be associated to different intermediary species of Ni during reduction. In general, the first peak at 375 °C is likely associated to reduction of Ni^{3+} to Ni^{2+}. The second and the third peaks are due to the reduction of Ni^{2+} into Ni^0, and a complete reduction is achieved at temperature 650 °C. This is in good agreement with XRD pattern for the $LaNiO_3$ sample as discussed in the next chapter below. In the literature both three [45,46] and two [47–49] step reduction behaviour has been reported in TPR for unsubstituted $LaNiO_3$ perovskite type samples. The maximum of first reduction peak at 375 °C in our study corresponds very well with the above literature findings. The ceria substitution clearly influences to the reduction behaviour of the $La_{1-x}Ce_xNiO_3$ samples. A slight shift of the peak maxima to lower temperatures was observed for samples with Ce substitution.

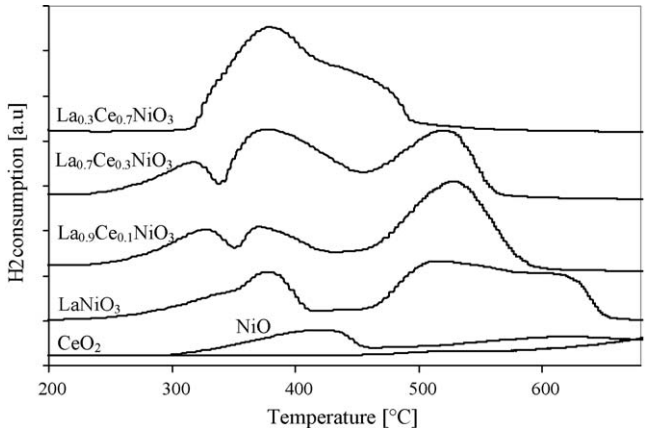

Fig. 3. The temperature-programmed reduction profiles for the $La_{1-x}Ce_xNiO_3$ catalysts with Ce substitution $x = 0$; 0.1; 0.3; 0.7 and with reference samples NiO and CeO_2. Reducing gas: 10% H_2 in He at 30 ml/min. The sample heating rate of 15 °C/min.

3.4. X-ray analysis and the size of Ni crystallites of the $La_{1-x}Ce_xNiO_3$ catalysts

The X-ray diffraction profiles of the calcined $La_{1-x}Ce_xNiO_3$ catalysts with substitution degrees of 0, 0.1, 0.3 and 0.7 are illustrated in Fig. 4a, and the respective catalysts after operation in Fig. 4b. The diffraction peaks around the 2θ angles of 37.4°, 43.2° and 63.0° are characteristic to nickel oxide, NiO [50]. All calcined, unused samples (Fig. 4a) show characteristic diffraction peaks of free NiO. The peak reflections due to NiO increased along the substitution degree of La with Ce indicating a higher content of NiO with higher Ce substitution. In the unsubstituted sample, $LaNiO_3$, peaks for perovskite type structure can be identified as well. However, the diffraction peaks characteristic to $LaNiO_3$ (23.4°, 32.8°, 47.2°) [51] weaken along the increasing substitution degree and cannot be identified any more in the catalyst with the highest substitution degree, $La_{0.3}Ce_{0.7}NiO_3$. For Ce substitution degree $x > 0.1$, the diffractogram displays lines which characteristic to cubic CeO_2 phase, but the 2θ angle positions of the peaks are shifted to smaller angles compared to those of the pure cubic CeO_2 phase with 2θ angles of 28.5°, 33.1° and 47.6°, 56.4° [52]. The observed peak shift might be attributed to the formation of mixed crystals, e.g. to the insertion of La^{3+} ions into the lattice of cerium oxide. This was confirmed with additional synthesis of Ni free La–Ce-oxides where the substitution degree of La with Ce was 0.0, 0.3, 0.5, 0.7 or 1.0. As seen in Fig. 4c, all the synthesized oxides containing Ce shows characteristic peaks to cubic crystal structure, but the insertion of La ions in the cubic structure CeO_2 causes peak position shift. The unsubstituted La_2O_3 showed the main diffractions in ranges which correspond to the hexagonal structure of the La_2O_3 lattice (26.1°, 29.1°, 30.0°, 39.5°, 46.1°, 52.1°) according to the corresponding PDF card from ICDD [53]. In the XRD analysis, no peaks characteristics to the reduced Ce_2O_3 (cubic or hexagonal) were detected (with main diffraction peak at 41.3 for cubic and 30.3 for hexagonal structure [54,55]).

The XRD patterns of the used $La_{1-x}Ce_xNiO_3$ catalysts (Fig. 4b) indicate that the NiO in the catalyst reduced to metallic Ni^0 during the reducing conditions in hydrogen treatment or operation. The diffraction peaks around the 2θ angles of 44.5°, 51.8° and 76.4° can be ascribed to metallic nickel, Ni^0. The size of Ni^0 crystallites was calculated according to the Scherrer equation from the diffractograms. The size of the crystallites was determined from one single peak at 2θ angle of 44.5° (Ni crystallite size 42, 26, 27 and 25 nm corresponding to the samples $LaNiO_3$, $La_{0.9}Ce_{0.1}NiO_3$, $La_{0.7}Ce_{0.3}NiO_3$ and $La_{0.3}Ce_{0.7}NiO_3$). These results indicate that the Ce substitution generally decreases the average size of Ni crystallite and improves the dispersion of Ni metal on the support, but the extent of the Ce substitution does not influence significantly on the average crystallite size.

The comparison of the XRD diffractograms of the fresh, calcined (unreduced) and the used $La_{1-x}Ce_xNiO_3$ materials reveal further changes in crystal structures of the investigated materials. The crystal structure of $La_{0.3}Ce_{0.7}NiO_3$ did not change noticeably during

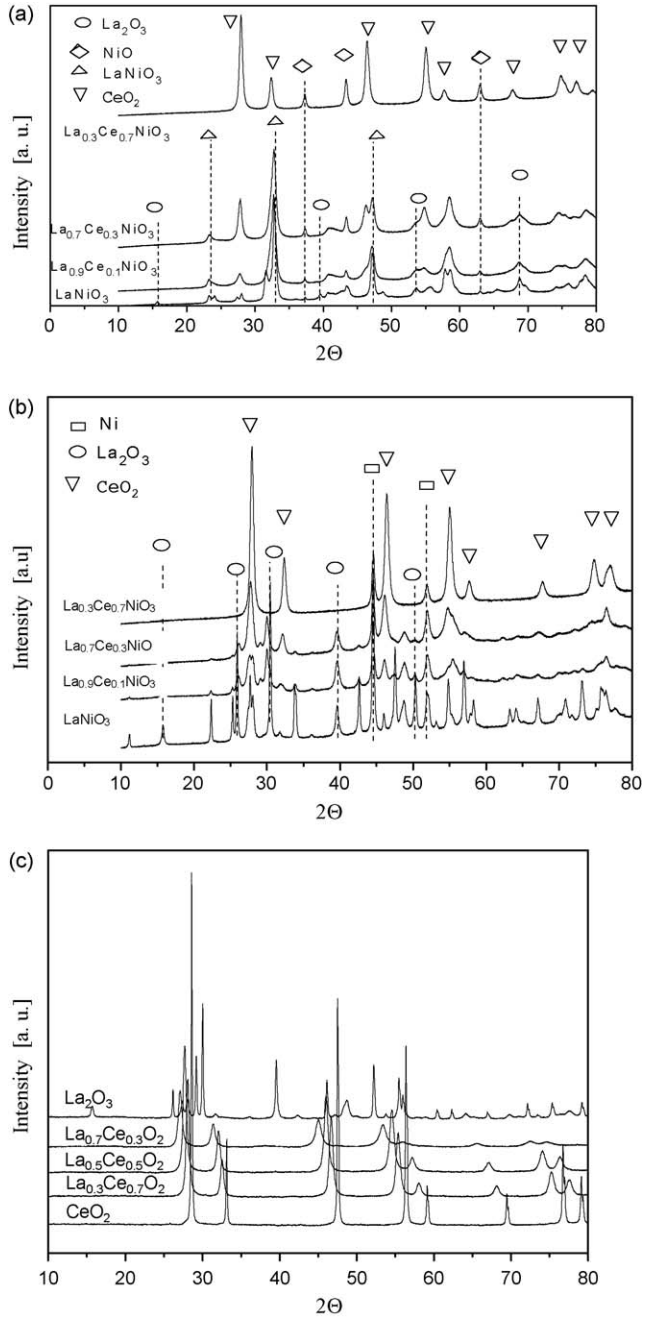

Fig. 4. The X-ray diffraction (XRD) profiles for the $La_{1-x}Ce_xNiO_3$ catalysts with Ce substitution $x = 0$; 0.1; 0.3; 0.7. (a) Fresh samples after calcination; (b) the used samples after the steam reforming of glycerol. (c) XRD profiles for substituted $La_{1-x}Ce_xO_2$, La_2O_3 and CeO_2.

the operation as the diffraction peak positions and the intensity ratio remained nearly unchanged, and the only rearrangement is the reduction of NiO to Ni^0 as confirmed by XRD. For the other mixed oxides, $LaNiO_3$, $La_{0.9}Ce_{0.1}NiO_3$ and $La_{0.7}Ce_{0.3}NiO_3$, more distinct diffraction peaks attributed to La_2O_3 could be detected for the used catalyst. Furthermore, the diffraction peaks attributed to $LaNiO_3$ were not any more detectable in any of the used catalyst, indicating the possible transformation of $LaNiO_3$ to Ni^0/La_2O_3 during the operation. Our observation of the phase segregation of the unsubstituted $LaNiO_3$ is in full agreement with the literature, where the instability of the $LaNiO_3$ structure has been reported both in the autothermal reforming of hydrocarbons and oxidative conversion of methane [56,57].

3.5. Influence of ceria substitution in $La_{1-x}Ce_xNiO_3$ in glycerol steam reforming

Finally, the activities of the Ce substituted $La_{1-x}Ce_xNiO_3$ catalyst were investigated in the steam reforming of glycerol. Because noble metal (Pt and Rh) catalysts have shown high activity in the autothermal reforming of various volatile hydrocarbons, e.g. glycerol [19], 3 wt% Pt metal catalysts on Y_2O_3 or mixed oxide carrier $Ce_{0.5}Zr_{0.5}O_2/10\%Y_2O_3$ were synthesized, and their activity was compared with that of the mixed oxides.

Prior to the catalyst activity studies, blank quartz reactor experiments were carried out in the temperature range between 500 and 700 °C. The conversion of glycerol was negligible at temperatures below 550 °C, but increased sharply from 2.4 to 33.6% at temperatures 600 and 700 °C. Small concentrations of gaseous products, e.g. CO, ethane and methane, were detected in the gas analysis during the blank quartz reactor tests but they were not further identified or quantified.

Fig. 5 illustrates the influence of temperature on the glycerol conversion into gaseous products with $La_{1-x}Ce_xNiO_3$ catalysts. Expectedly, the glycerol conversion was found to increase with increasing temperature, as reported in the previous studies with various catalysts [13–17]. The Ce substitution in the $La_{1-x}Ce_xNiO_3$ catalyst influenced remarkably on the conversion, whereas the activity differences were most pronounced at the temperatures 500 and 550 °C. The catalyst with the substitution level of 0.7, $La_{0.3}Ce_{0.7}NiO_3$, showed >98% conversion to gaseous products at each investigated temperature (see Fig. 5), and the conversion was very close to the thermodynamic equilibrium value in all investigated temperatures. The noble metal catalyst Pt/Y_2O_3 showed comparable activity to the $La_{0.3}Ce_{0.7}NiO_3$. As seen in the figure, at 600 °C the conversion of glycerol to gaseous products was between 60 and 95% with the other investigated catalysts. At 700 °C all tested catalysts showed high activity, and nearly complete conversion to gaseous products was obtained. Furthermore, it should be mentioned here that at 600 °C the *overall* conversion of glycerol was complete with all tested catalysts, as no glycerol was analyzed in the liquid product sample by the HPLC. This indicates that at 600 °C glycerol was decomposed, but the products were not completely gaseous at this temperature. As a summary, the activity of the catalyst in the steam reforming of

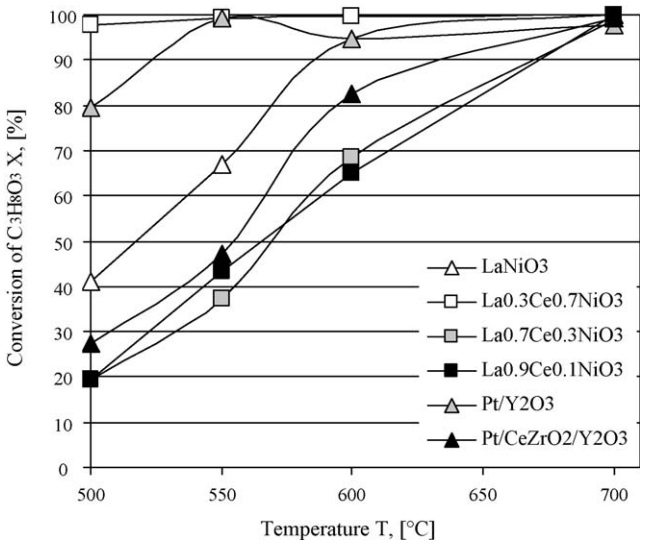

Fig. 5. The influence of temperature on the glycerol conversion to gaseous products with $La_{1-x}Ce_xNiO_3$ and the Pt-based catalysts. Experimental conditions: H_2O–glycerol–liquid flow rate 0.06 ml/min, H_2O/glycerol molar ratio 24, carrier gas Ar 33 ml/min.

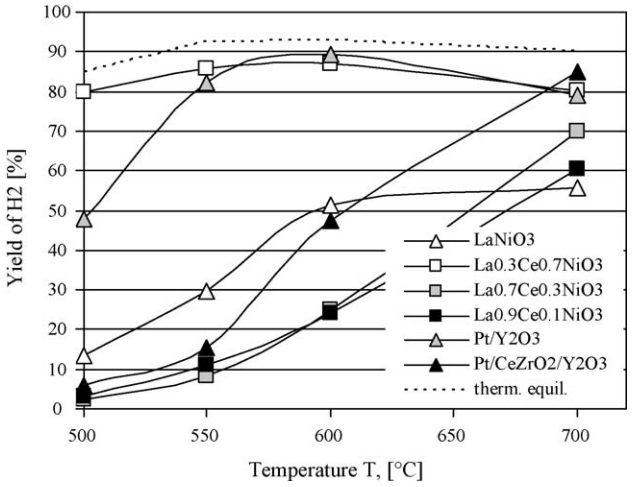

Fig. 6. The influence of temperature on the yield of hydrogen with $La_{1-x}Ce_xNiO_3$ and the Pt-based catalysts. Experimental conditions: H_2O–glycerol–liquid flow rate 0.06 ml/min, H_2O/glycerol molar ratio 24, carrier gas Ar 33 ml/min.

glycerol followed the order: $La_{0.3}Ce_{0.7}NiO_3 \approx Pt/Y_2O_3 > LaNiO_3 > Pt/CeZrO_2/Y_2O_3 > La_{0.9}Ce_{0.1}NiO_3 \approx La_{0.7}Ce_{0.3}NiO_3$.

The hydrogen yield was dependent on the temperature as illustrated in Fig. 6. The hydrogen yield increased steadily as a function reaction temperature with the catalysts $LaNiO_3$, $La_{0.9}Ce_{0.1}NiO_3$, $La_{0.7}Ce_{0.3}NiO_3$ and $Pt/CeZrO_2/Y_2O_3$. The hydrogen yield with the two most active catalysts, $La_{0.3}Ce_{0.7}NiO_3$ and Pt/Y_2O_3, was considerably higher than that with the other catalyst already at 500 and 550 °C, and especially with $La_{0.3}Ce_{0.7}NiO_3$ the hydrogen yield was closely to the thermodynamic equilibrium yield over the whole investigated temperature range. The influence of the thermodynamic equilibrium explains the decreasing tendency of hydrogen yield with the two most active catalysts at temperatures above 600 °C. This decreasing tendency of hydrogen yield with the highly active catalysts is in agreement with the results of Adhikari et al. [15]. The highest yield of hydrogen at 600 °C with the catalysts $La_{0.3}Ce_{0.7}NiO_3$ and Pt/Y_2O corresponds to the approximate formation rate of hydrogen 1500 μmol min^{-1} g^{-1}.

The fractional conversions to the carbon containing components CO_2, CO and CH_4 are presented at temperatures 500, 550, 600 and 650 °C in Fig. 7a–d. In Fig. 7, the fractional conversion to CO is illustrated as the difference between the two lowest lines (symbols

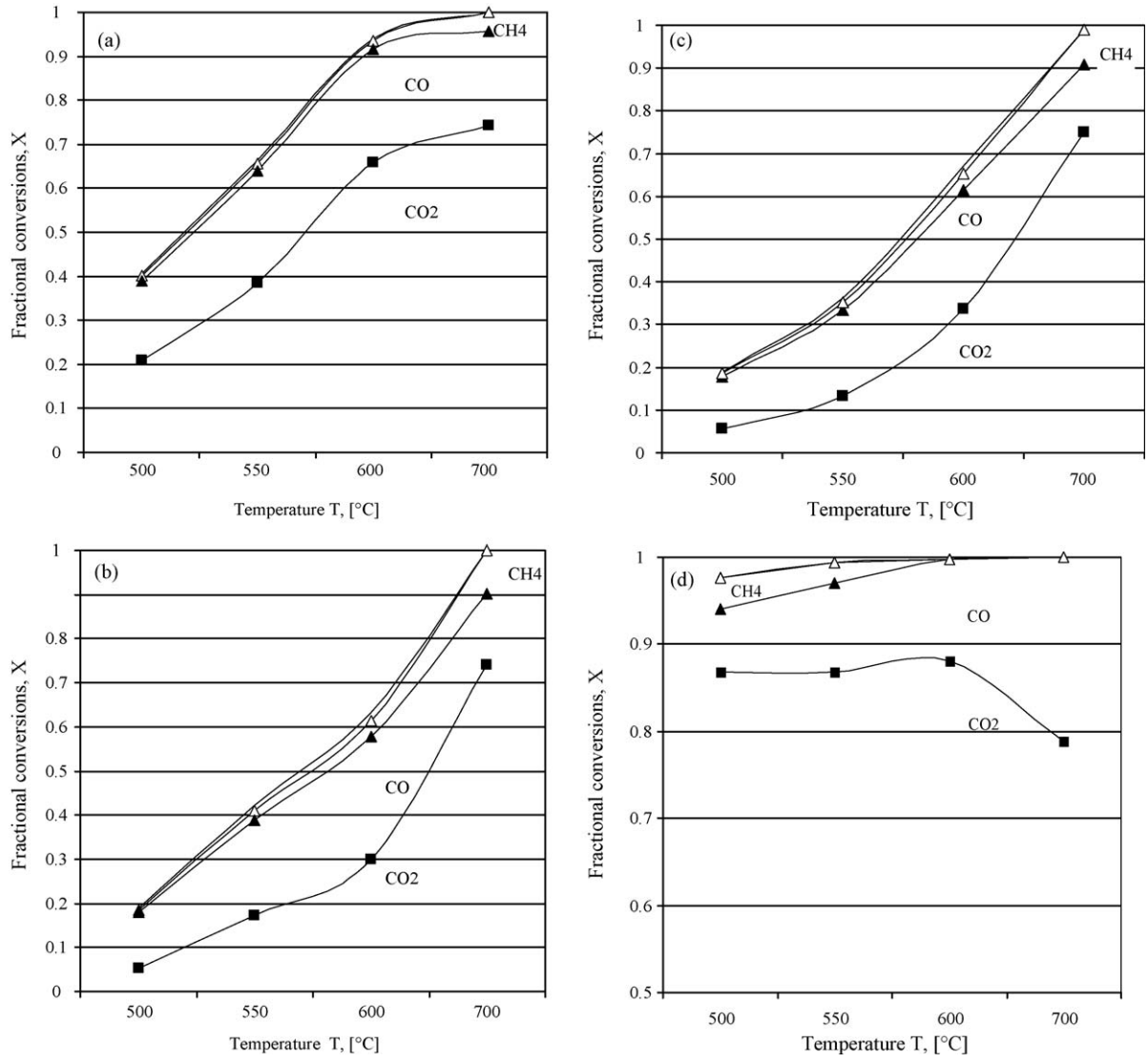

Fig. 7. (a–d) The influence of temperature on the fractional conversions to CO_2, CO, and CH_4 with (a) $LaNiO_3$, (b) $La_{0.9}Ce_{0.1}NiO_3$, (c) $La_{0.7}Ce_{0.3}NiO_3$ and (d) $La_{0.3}Ce_{0.7}NiO_3$ Experimental conditions: H_2O–glycerol–liquid flow rate 0.06 ml/min, H_2O/glycerol molar ratio 24, carrier gas Ar 33 ml/min.

■ and ▲), the fractional conversion to CH_4 as the difference between the lines with symbols ▲ and △. The fractional conversion to CO_2 with catalysts with the substitution levels of $x = 0$, 0.1 and 0.3, increased clearly as a function of temperature (see Fig. 7a–c). With $La_{0.3}Ce_{0.7}NiO_3$ the fractional conversion to CO_2 were at very high level over the whole investigated temperature range (see Fig. 7d, please remark different ordinate scale). Due to the reaction equilibrium of the water-gas-shift reaction (WGS, Eq. (6)), the CO_2 formation was depressed at high temperatures, which was observed also experimentally as the fractional conversion to CO_2 was found to decrease at temperatures above 600 °C with the most active catalysts $La_{0.3}Ce_{0.7}NiO_3$. For the other catalysts, the influence of the thermodynamic equilibrium was not so intensive due to the limited activity of the materials, and the conversion levels were generally considerably lower than with the most active catalysts. At the low temperature range (500–600 °C) the fractional conversion to CO_2 with the various catalysts followed the same order as reported above for the hydrogen yield: $La_{0.3}Ce_{0.7}NiO_3 > LaNiO_3 > La_{0.9}Ce_{0.1}NiO_3 \approx La_{0.7}Ce_{0.3}NiO_3$. At the temperature 700 °C the system was likely controlled by the thermodynamic equilibria with all the catalysts and the fractional conversions to CO_2 were between 75 and 80%.

Interesting differences between the fractional conversions to CO and CO_2 can be seen in Fig. 7a–d. At temperatures below 600 °C, all the catalysts showed closely similar fractional conversions to CO. However, the catalysts $La_{0.9}Ce_{0.1}NiO_3$ and $La_{0.7}Ce_{0.3}NiO_3$ showed clearly lower fractional conversion to CO_2 in this temperature range which indicates that these catalysts are highly active in the reforming reaction, but the activity in the subsequent water-gas-shift reaction is limited. The $La_{0.3}Ce_{0.7}NiO_3$ showed high activity in the WGS even at the low temperature range which was observed as high fractional conversion to CO_2. With the $La_{0.3}Ce_{0.7}NiO_3$ catalyst the fractional conversions followed closely the thermodynamic equilibrium values, and at higher temperatures the fractional conversion to CO increased due the WGS reaction equilibrium.

The fractional conversions to CH_4 are illustrated in Fig. 7 as well. At 500 °C, only $La_{0.3}Ce_{0.7}NiO_3$ showed clear fractional conversion to CH_4 whereas with the other catalysts the fractional conversion to CH_4 was negligible. At temperature above 550 °C the fractional conversion to CH_4 decreased with the most active catalysts, $La_{0.3}Ce_{0.7}NiO_3$ which is in full accordance with our thermodynamic estimations. The selectivity of CH_4 increased along the reaction temperature with the catalyst $La_{0.9}Ce_{0.1}NiO_3$ and $La_{0.7}Ce_{0.3}NiO_3$ at temperatures between 500 and 700 °C.

The fractional conversion to C_2 compounds (C_2H_4 and C_2H_6) during the glycerol steam reforming was followed as well. With the most active catalyst, $La_{0.3}Ce_{0.7}NiO_3$ the fractional conversion to C_2 compounds was negligible at the whole temperature range. The fractional conversion to C_2 compounds was observed with catalysts of the substitution levels $x = 0.1$ or 0.3 at temperatures 550 and 600 °C, but it remained always <0.018 in all tested conditions. At 700 °C, selectivity to C_2 was not observed with any catalyst which indicates that all C_2 compounds were converted at high temperatures.

Finally, the operational stability of the most active catalyst $La_{0.3}Ce_{0.7}NiO_3$ was tested at 600 °C during 10 h test. The catalytic activity remained unchanged during the 10 h investigation, and no change in the conversion or in the hydrogen yield was observed.

4. Conclusions

Partially Ce substituted $La_{0.3}Ce_{0.7}NiO_3$ mixed oxide showed high activity and stability in the glycerol steam reforming. The activity was comparable to that of a noble metal (Pt). The $La_{0.3}Ce_{0.7}NiO_3$ remained stable during the initial 10-h test for the reforming reaction. Unchanged catalyst surface area (BET) during operation and low carbon deposition after reaction confirms the efficient operation and high stability of this non-noble, inexpensive catalyst $La_{0.3}Ce_{0.7}NiO_3$.

Acknowledgement

Dr. Y. Cui is grateful for the support of a Max Planck Scholarship funded by the Max Planck Gesellschaft.

References

[1] F. Orecchini, E. Bocci, Energy 32 (2007) 1006–1011.
[2] A. Haryanto, S. Fernando, N. Murali, S. Adhikari, Energy Fuels 19 (2005) 2098–2106.
[3] S.A. Sherif, F. Barbir, T.N. Veziroglu, Sol. Energy 78 (2005) 647–660.
[4] E. Bilgen, Sol. Energy 77 (2004) 47–55.
[5] V. Galvita, K. Sundmacher, Appl. Catal. A: Gen. 289 (2005) 121–127.
[6] P. Ramirez de la Piscina, N. Homs, Chem. Soc. Rev. 37 (2008) 2459–2476.
[7] D.T. Johnson, K.A. Taconi, Environ. Prog. 26 (2007) 338–348.
[8] A. Behr, J. Eilting, K. Irawadi, J. Leschinski, F. Lindner, Green Chem. 10 (2008) 13–30.
[9] R.D. Cortright, R.R. Davda, J.A. Dumesic, Nature 418 (2002) 964–967.
[10] G.W. Huber, J.W. Shabaker, J.A. Dumesic, Science 300 (2003) 2075–2077.
[11] J.W. Shabaker, G.W. Huber, J.A. Dumesic, J. Catal. 222 (2004) 180–191.
[12] H. Hori, K. Koike, Y. Sakai, H. Murakami, K. Hayashi, K. Nomiya, Energy Fuel 19 (2005) 2209–2213.
[13] D.A. Simonetti, E.L. Kunkes, J.A. Dumesic, J. Catal. 247 (2007) 298–306.
[14] S.M. Swami, M.A. Abraham, Energy Fuels 20 (2006) 2616–2622.
[15] S. Adhikari, S. Fernando, A. Haryanto, Energy Fuels 21 (2007) 2306–2310.
[16] S. Adhikari, S. Fernando, A. Haryanto, Catal. Today 129 (2007) 355–364.
[17] B. Zhang, X. Tang, Y. Li, Y. Xu, W. Shen, Int. J. Hydrogen Energy 32 (2007) 2367–2373.
[18] A.M.D. Douette, S.Q. Turn, W. Wang, V.I. Keffer, Energy Fuel 21 (2007) 3499–3504.
[19] T. Hirai, N.O. Ikenaga, T. Miyake, T. Suzuki, Energy Fuel 19 (2005) 1761–1762.
[20] P.J. Dauenhauer, J.R. Salge, L.D. Schmidt, J. Catal. 244 (2006) 238–247.
[21] A. Houteit, H. Mahzoul, P. Ehrburger, P. Bernhardt, P. Légaré, F. Garin, Appl. Catal. A: Gen. 306 (2006) 22–28.
[22] G. Busca, U. Costantino, F. Marmottini, T. Montanari, P. Patrono, F. Pinzari, G. Ramis, Appl. Catal. A: Gen. 310 (2006) 70–78.
[23] C. Qi, J.C. Amphlett, B.A. Peppley, Appl. Catal. A: Gen. 302 (2006) 237–243.
[24] T. Tanabe, S. Kameoka, A.P. Tsai, Catal. Today 111 (2006) 153–157.
[25] C.-Z. Yao, L.-C. Wang, Y.-M. Liu, G.-S. Wu, Y. Cao, W.-L. Dai, H.-Y. He, K.-N. Fan, Appl. Catal. A: Gen. 297 (2006) 151–158.
[26] S. Patel, K.K. Pant, J. Power Sources 159 (2006) 139–143.
[27] M.N. Barroso, M.F. Gomez, L.A. Arrúa, M.C. Abello, Appl. Catal. A: Gen. 304 (2006) 116–123.
[28] H.-S. Roh, Y. Wang, D.L. King, A. Platon, Y.-H. Chin, Catal. Lett. 108 (1–2) (2006) 15–19.
[29] A. Casanovas, J. Llorca, N. Homs, J.L.G. Fierro, P.R. de la Piscina, J. Mol. Catal. A: Chem. (2006) 44–49.
[30] Y. Yang, J. Ma, F. Wua, Int. J. Hydrogen Energy 31 (2006) 877–882.
[31] H.V. Fajardo, L.F.D. Probst, Appl. Catal. A: Gen. 306 (2006) 134–141.
[32] N. Laosiripojana, S. Assabumrungrat, Appl. Catal. B: Environ. 66 (2006) 29–39.
[33] H.-S. Roh, A. Platon, Y. Wang, D.L. King, Catal. Lett. 110 (1–2) (2006) 1–6.
[34] B. Zhang, X. Tang, Y. Li, W. Cai, Y. Xu, W. Shen, Catal. Commun. 7 (2006) 367–372.
[35] V.V. Galvita, G.L. Semin, V.D. Belyaev, V.A. Semikolenov, P. Tsiakaras, V.A. Sobyanin, Appl. Catal. A: Gen. 220 (2001) 123–127.
[36] E.C. Wanat, K. Venkataraman, L.D. Schmidt, Appl. Catal. A: Gen. 276 (2004) 155–162.
[37] S. Velu, K. Suzuki, M. Vijayaraj, S. Barman, C.S. Gopinath, Appl. Catal. B: Environ. 55 (2005) 287–299.
[38] V. Mas, R. Kipreos, N. Amadeo, M. Laborde, Int. J. Hydrogen Energy 31 (2006) 21–28.
[39] Y. Lwin, W.R.W. Daud, A.B. Mohamad, Z. Yaakob, Int. J. Hydrogen Energy 25 (2000) 47–53.
[40] K. Faungnawakij, R. Kikuchi, K. Eguchi, J. Power Sources 161 (2006) 87–94.
[41] R.H. Perry, D.W. Green, J.O. Maloney, Perry's Chemical Engineers' Handbook, McGraw-Hill, New York, 1997.
[42] R.C. Reid, J.M. Prausnitz, B.E. Poling, The Properties of Gases and Liquids, 4th ed., McGraw Hill Book, Singapore, 1988.
[43] J.A. Dean, Lange's Handbook of Chemistry, 15th ed., McGraw Hill, New York, 1999
[44] S. Adhikari, S. Fernando, S.R. Gwaltney, S.D.F. To, R.M. Bricka, P.H. Steele, A. Haryanto, Catal. Today 129 (2007) 355–364.
[45] G. Valderrama, M.R. Goldwasser, C.U. de Navarro, J.M. Tatibouët, J. Barrault, C. Batiot-Dupeyrat, F. Martínez, Catal. Today 107 (108) (2005) 785–791.
[46] M.E. Rivas, J.L.G. Fierro, R. Guil-López, M.A. Peña, V. La Parola, M.R. Goldwasser, Catal. Today 133 (135) (2008) 367–373.
[47] S.M. Lima, J.M. Assaf, M.A. Peña, J.L.G. Fierro, Appl. Catal. A: Gen. 311 (2006) 94–104.
[48] S. Utsumi, F.E. Vallejos-Burgos, C.M. Campos, X. García, A.L. Gordon, G. Pecchi, L.R. Radovic, Catal. Today 123 (2007) 208–217.

[49] G.C. de Araujo, S.M. de Lima, J.M. Assaf, M.A. Peña, J.L.G. Fierro, M.C. Rangel, Catal. Today 133 (135) (2008) 129–135.
[50] International Centre for Diffraction Data (ICDD), PDF of NiO, reference code 01-089-7390, 2003.
[51] International Centre for Diffraction Data (ICDD), PDF of $LaNiO_3$, reference code 00-010-0341, 2003.
[52] International Centre for Diffraction Data (ICDD), PDF of CeO_2, reference code 03-065-5923, 2003.
[53] International Centre for Diffraction Data (ICDD), PDF of La_2O_3, reference code 01-74-2430, 2003.
[54] International Centre for Diffraction Data (ICDD), PDF of cubic Ce_2O_3, reference code 00-049-1458, 2003.
[55] International Centre for Diffraction Data (ICDD), PDF of hexagonal Ce_2O_3, reference code 00-023-1048, 2003.
[56] V.R. Choudhary, B.S. Uphade, A.A. Belhekar, J. Catal. 163 (1996) 312–318.
[57] J.R. Mawdsley, T.R. Krause, Appl. Catal. A: Gen. 334 (2008) 311–320.